

Article

# Synthesis of Porous ZnO Nanosheets and Carbon Nanotube Hybrids as Efficient Photocatalysts via Pulsed Laser Ablation

Yun Yeol Ryu, Taekyung Kim and HyukSu Han \*

Department of Materials Science and Engineering, Hongik University, Sejong-ro 2639, Korea

\* Correspondence: hhan@hongik.ac.kr

Received: 3 September 2019; Accepted: 20 September 2019; Published: 21 September 2019



**Abstract:** Zinc oxide (ZnO) has attractive photocatalytic properties. However, the high recombination rate of the photo-excited charge carriers on this material often restricts application. Here, we report that hybridization of one dimensional (1D) carbon nanotubes (CNT) on two dimensional (2D) porous ZnO nanosheets (NS) can be a promising strategy to overcome some of the challenges of ZnO. Specifically, a pulsed laser ablation technique was utilized to hybridize 1D CNT with 2D porous ZnO NS in environmentally friendly as well as super-economic (short time, less than 10 min) conditions. The synthesized ZnO NS-CNT hybrids show a significantly enhanced photocatalytic activity for water splitting relative to their counterpart ZnO NS.

**Keywords:** photocatalyst; water splitting; zinc oxide; carbon nanotube; pulsed laser ablation; nanocomposites

## 1. Introduction

Photoelectrochemical (PEC) water splitting for hydrogen production has attracted great attention as clean and sustainable energy conversion technology after Fujishima and Honda first reported the hydrogen evolution reaction (HER) of  $\text{TiO}_2$  via PEC water splitting [1,2]. Novel metal-based materials such as platinum (Pt), iridium (Ir), and ruthenium (Ru) are the most efficient catalysts for hydrogen production. However, their scarcity and high cost hinders the practical applications of novel metal-based catalysts towards mass production of hydrogen [3,4]. Therefore, tremendous efforts have been made on the development of earth-abundant and low-cost alternatives with excellent photocatalytic activity.

ZnO is regarded as a promising photocatalyst due to high electron mobility at room temperature, easy control of nanostructures, low-cost, and non-toxicity [5]. However, a wide band gap and high recombination rate have limited ZnO as a high-performance photocatalyst in wide applications. Notably, highly conductive co-catalysts can effectively suppress charge recombination by modifying the electronic configuration of primary catalysts and prolong carrier lifetime. Carbon-based materials such as carbon nitride, graphene, or carbon nanotube (CNT) are some of the most promising co-catalysts thanks to excellent charge transport, high surface area, robustness, and low-cost. Hence, various hybrids comprised of semiconductive photocatalyst and conductive carbon materials have been intensively studied with an aim to replace expensive novel metal-based catalysts for water splitting [6–8].

Wet-chemical routes are conventionally used to synthesize carbon-based composite materials, which often leaves acidic residues that needs to be purified for further application [9,10]. The synthesis of nanomaterials by pulsed laser ablation (PLA) has attracted significant attention [11–14]. PLA is able to downsize bulk particles into nanometer-sized structures within a few minutes. More importantly, PLA does not need to utilize highly acidic (e.g.,  $\text{KMnO}_4$ ,  $\text{H}_2\text{SO}_4$ ) or basic aqueous solutions (e.g.,  $\text{KOH}$ ,

HNO<sub>3</sub>) [10,15–17]. Hence, PLA can be employed to synthesize nanocomposites in environmentally friendly and cost-effective way. PLA has been rarely studied for preparing high-performance photocatalytic nanocomposites due to its high potential. In addition, nanocomposites of ZnO and carbon based materials for photocatalysis have often been prepared via wet-chemical routes, which requires prolong synthesis time and multiple steps [18–22]. To the best of our knowledge, it is first time that ZnO and carbon based nanocomposites for photoelectrochemical water splitting using a facile and cost-effective PLA technique have been developed.

Herein, we report a novel strategy to develop efficient photocatalytic ZnO nanosheets (ZnO NS) hybridized with carbon materials by using a PLA technique. We investigated the modulation of PEC properties of ZnO NS after carbon hybridization via PLA. Photocatalytic activity of ZnO NS was significantly enhanced after only 10 min of PLA process in water, resulting in homogeneously distributed carbon nanotubes (CNTs) on the surface of the ZnO NS. Based on the results, it was demonstrated that PLA is a highly promising technique to prepare efficient photocatalytic nanocomposites, especially with carbon-based materials.

## 2. Results and Discussion

Figure 1 shows field-emission scanning electron microscopy (FE-SEM) images of ZnO NS before calcination. As-prepared ZnO NS has a well-defined nanosheet structure with high surface area. After calcination, the morphology of the as-prepared ZnO NS became highly porous surface morphology which can be beneficial for enhancing photocatalytic activity (Figure 2a). As a control experiment, ZnO NS was physically mixed with CNT; the SEM image is shown in Figure 2b. Aggregated tubular CNT was found on the surface of ZnO NS. In contrast, after PLA process for 1 min, the CNT aggregates were not observed, indicating that successful ablation was achieved within 1 min of PLA processing (Figure 2c). Interestingly, for further ablation (5 and 10 min), ZnO NS was partially converted to round shape ZnO nanoparticles (NPs) (Figure 2d–e) with well dispersed CNT. However, when the ablation time was increased up to 30 min, large amount of ZnO NP instead of ZnO NS was formed and no CNT was observed (Figure 2f). This implies that CNT was completely transformed to graphene quantum dots (GQD) during the PLA process. In addition, PLA can facilitate the transformation of ZnO NS to NP, resulting in significant morphology change after PLA for 30 min. We also investigated the effect of laser wavelengths on the structural change of ZnO NS and CNT (ZnO NS-CNT) hybrids. Figure 3 shows the SEM image of the ZnO NS-CNT hybrid ablated by a laser with longer wavelengths (532 nm) for 10 min. It was found that large amounts of CNT aggregates were still remaining on the surface of ZnO NS. Also, morphology change from ZnO NS to NP was not detected, indicating that sufficient laser energy is necessary to control the morphology of CNT or ZnO NS by PLA process.

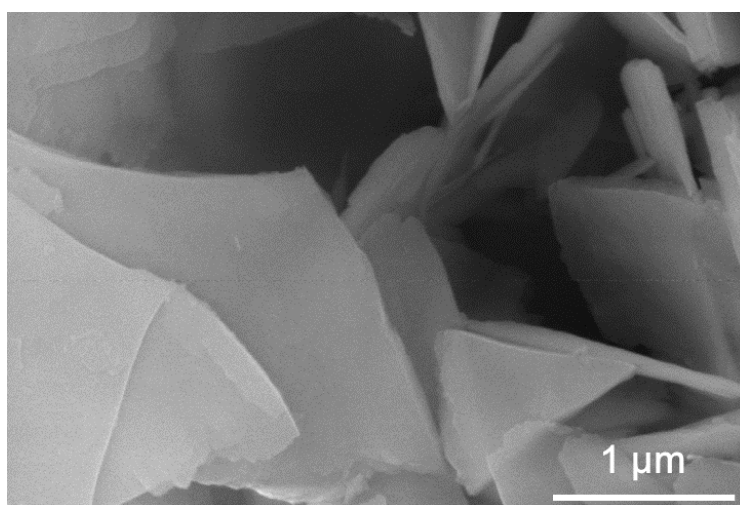


**Figure 1.** Scanning electron microscopy images for as-prepared ZnO NS before calcination.

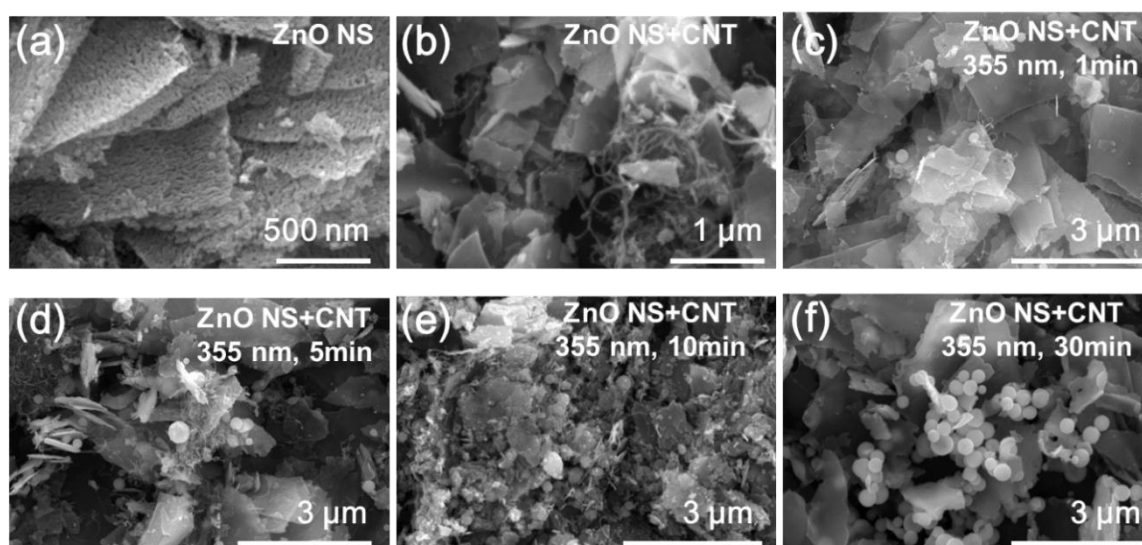


**Figure 2.** Scanning electron microscopy images for as-prepared (a) ZnO NS, (b) ZnO NS-CNT, (c) ZnO NS-CNT (355 nm, 1 min), (d) ZnO NS-CNT (355 nm, 5 min), (e) ZnO NS-CNT (355 nm, 10 min), and (f) ZnO NS-CNT (355 nm, 30 min).

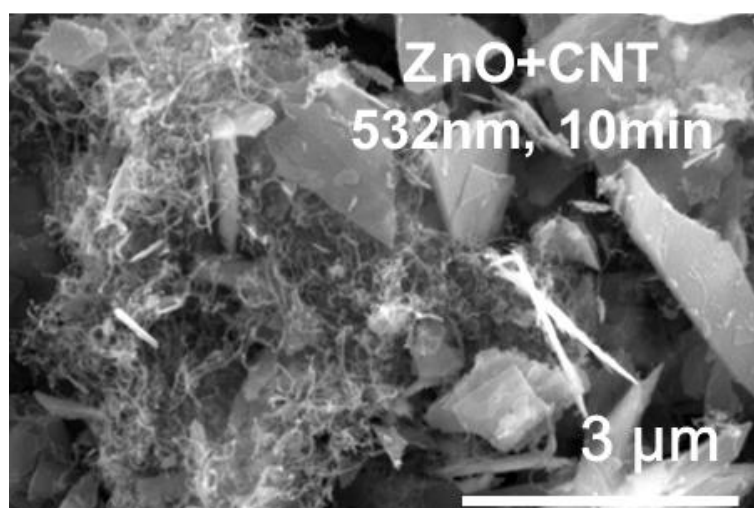


**Figure 3.** Scanning electron microscopy images for ZnO NS-CNT (532 nm, 10 min).

Crystallographic structure of the ZnO NS-CNT hybrids was studied by XRD. The XRD patterns of all samples (ZnO NS, ZnO NS-CNT, ZnO NS-CNT (1 min), ZnO NS-CNT (5 min), ZnO NS-CNT (10 min), and ZnO NS-CNT (30 min)) are shown in Figure 4. Notably, the XRD patterns were well-matched with the standard XRD pattern (PDF# 01-078-3325) of the ZnO phase. The formation of the hexagonal wurtzite structure of ZnO was confirmed since the diffracted peaks at 31.85, 34.42, 36.30, 47.58, 56.73, 62.87, and 68.11° can be indexed along the (010), (002), (011), (012), (110), (013), and (112) planes of the phase. No secondary phases were observed for ZnO NS or ZnO NS-CNT hybrids demonstrating that the PLA process has the advantage of preparing ZnO and carbon composites with a controlled crystal phase and structure within a very short time. Nitrogen adsorption–desorption isotherm was performed for the ZnO NS and ZnO NS-CNT hybrid to estimated surface area. As shown in Figure 5, BET surface areas of 23.31 and 34.62 m<sup>2</sup>g<sup>−1</sup> were measured for ZnO NS and ZnO NS-CNT hybrids, respectively. Interestingly, the BET surface area was slightly increased after hybridization, possibly due to the partially ablated CNT tubular structure. The larger surface area of ZnO NS-CNT hybrid may be beneficial for enhancing photocatalytic activity by facilitating mass or charge transport during electrolysis.

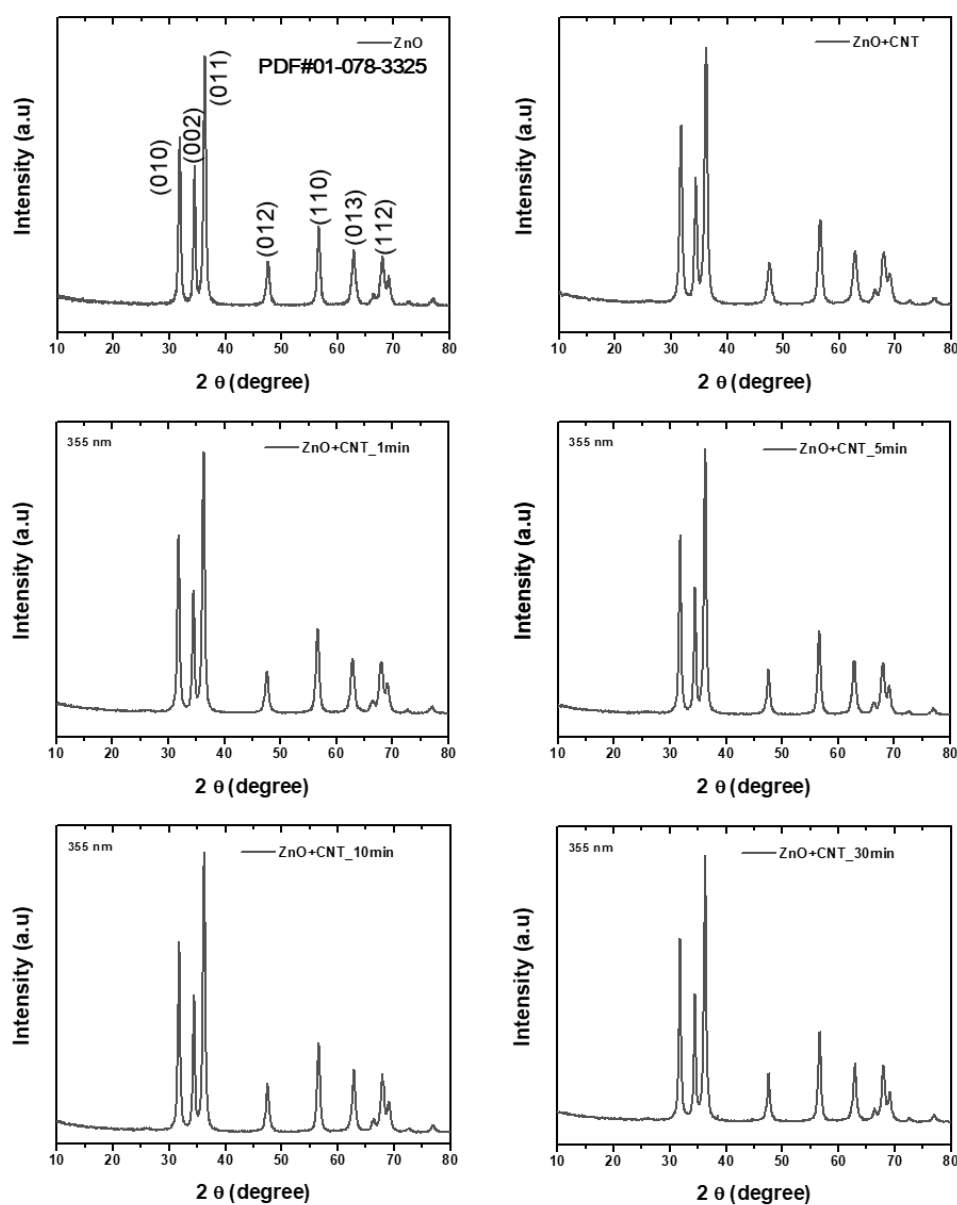


Figure 4. XRD patterns of ZnO NS and ZnO-CNT hybrids prepared in different PLA conditions.

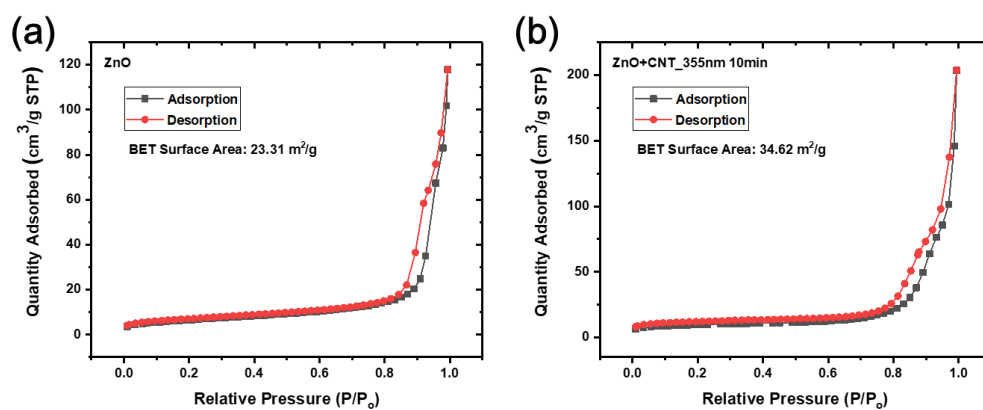


Figure 5.  $N_2$  adsorption–desorption isotherm for measuring Brunauer–Emmett–Teller surface areas of (a) ZnO NS and (b) ZnO NS-CNT (355 nm, 10 min), respectively. Black and red lines represent adsorption and desorption data, respectively.

Transmission electron microscopy (TEM) was utilized to investigate structural characterization of as-synthesized ZnO NS and ZnO NS-CNT hybrids. Figure 6a shows low-resolution TEM images of ZnO NS, where two dimensional (2D) porous nanosheet structure is clearly observed. High-resolution TEM (HR-TEM) with corresponding selective area electron diffraction (SAED) images revealed that the synthesized ZnO NS has polycrystalline structure crystallized in a distinct hexagonal wurtzite ZnO phase (Figure 6b). Energy dispersive X-ray (EDX) spectroscopy was performed in order to acquire elemental distributions in the sample. Figure 6c,d shows EDX mapping images for Zn and O in the ZnO NS sample, respectively, where homogeneous elemental distributions are clearly presented. In addition, quantitative EDX spectra analysis demonstrated that Zn and O have atomic ratios of about 1:1, which is inconsistent with XRD and TEM results (Figure 6e). Figure 7 shows the HR-TEM images of the ZnO-CNT hybrid after a 10 min PLA process. The distinct 2D porous nanosheet structure had remained after the PLA process (Figure 7a). Furthermore, the formation of the ZnO NS and CNT hybrid was clearly observed, as shown in Figure 7b; a lattice fringe of 2.59 Å, corresponding to (002) of ZnO, was presented in junction with that of the layered CNT (lattice fringe of 4.14 Å).

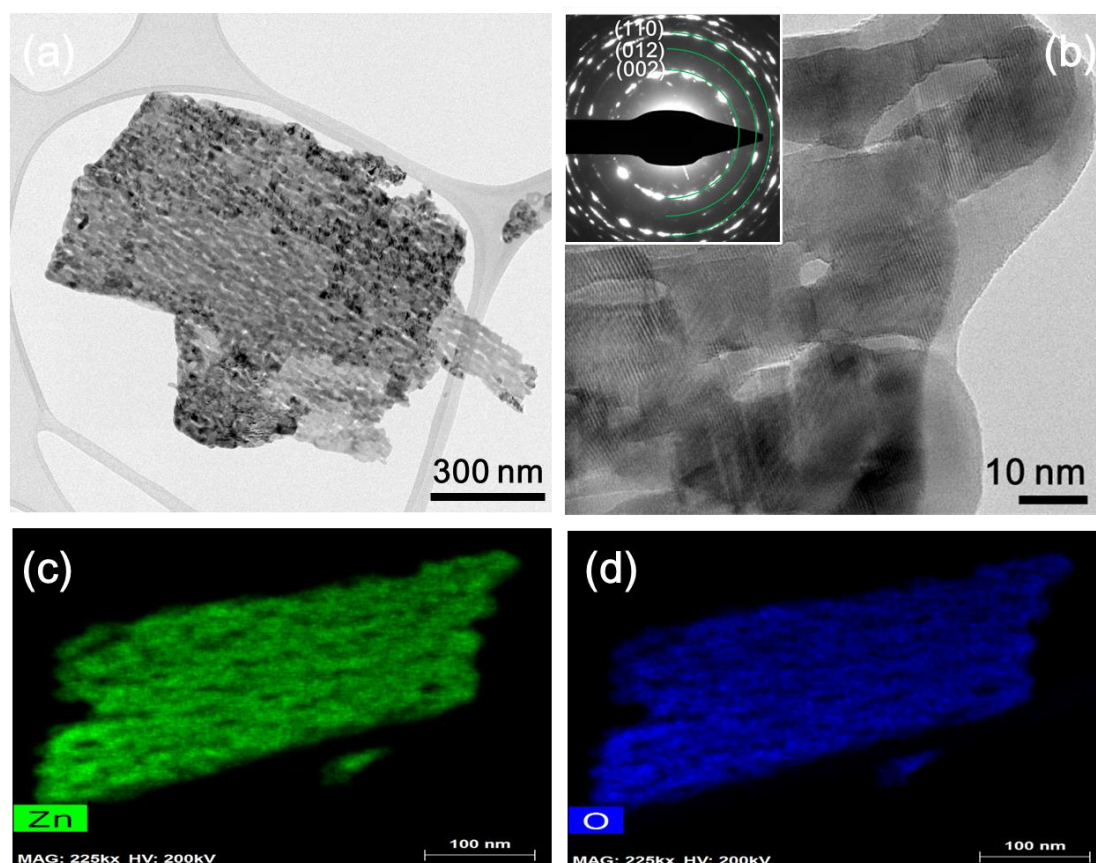
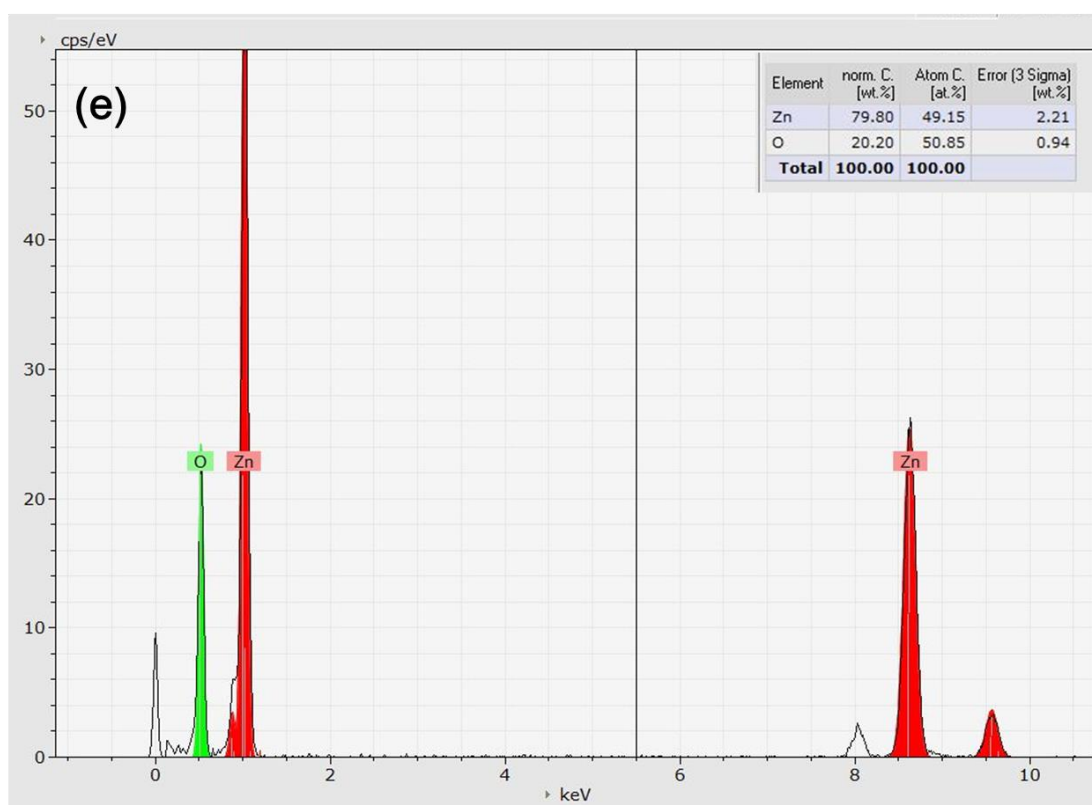
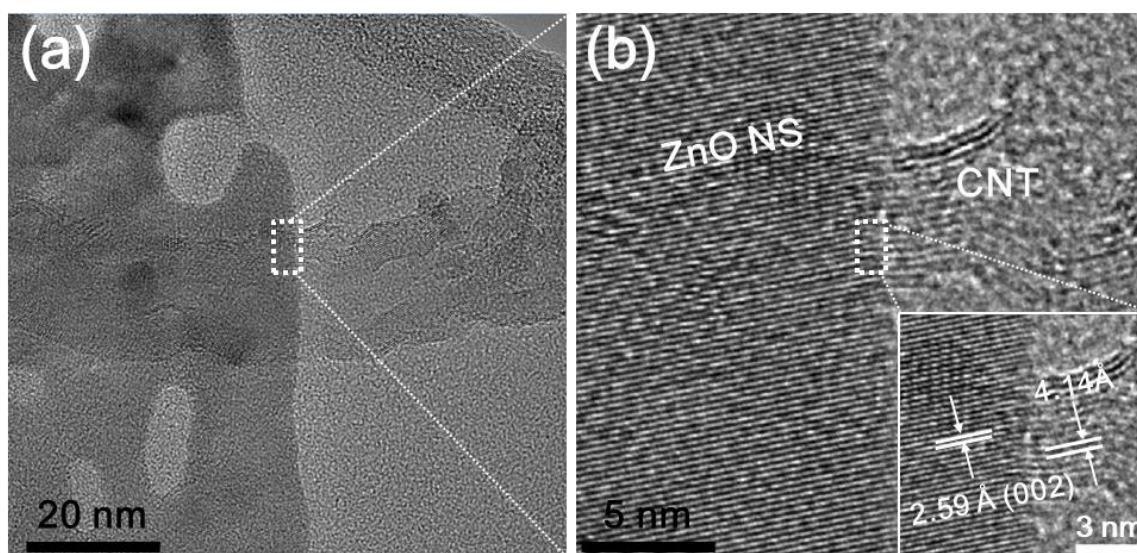


Figure 6. Cont.



**Figure 6.** (a) Low-resolution transmission electron microscopy image of ZnO NS after calcination. (b) High-resolution transmission electron microscopy image of ZnO NS (upper insets show the selective area electron diffraction pattern). (c,d) Energy dispersive X-ray mapping images of ZnO NS for Zn and O, respectively. (e) Quantitative EDX spectroscopy data for ZnO NS.



**Figure 7.** (a) High-resolution transmission electron microscopy image of ZnO NS-CNT (355 nm, 10 min) hybrid, where (b) clear lattice fringes of ZnO is presented in contact with that of CNT.

#### Photoelectrochemical Characterization

The transient photocurrents of the samples were measured under on/off illumination cycles. Figure 8 shows that ZnO NS-CNT hybrids exhibit reproducible and immediate responses to irradiation. The photocurrent of samples rapidly increases to the maximum value under light, and it immediately

drops to near-zero when the light is switched off. The photocurrent of ZnO NS is around  $20 \mu\text{A cm}^{-2}$  while that of ZnO NS-CNT hybrids are about 2–4 times higher. The enhanced photocurrents of ZnO NS-CNT hybrids can be related to the improved charge transport via highly conductive CNTs. As the ablation time increases up to 10 min, the PEC performance of the ZnO NS-CNT hybrid was enhanced, and reached the highest photocurrent ( $120 \mu\text{A cm}^{-2}$ ). However, for further ablation, the photocurrent of the sample was abruptly decreased. The ZnO NS-CNT hybrid ablated for 60 min exhibited significantly lower photocurrent ( $3 \mu\text{A cm}^{-2}$ ) than that of pristine ZnO NS ( $20 \mu\text{A cm}^{-2}$ ). These results indicate that the formation of ZnO NP may not be helpful for enhancing PEC performance of ZnO-CNT hybrids. In addition, well dispersed CNTs onto ZnO NS is important to achieve high photocatalytic activity of the ZnO-CNT hybrid. In addition, the ZnO-CNT hybrid ablated for 10 min using the laser with the wavelength of 532 nm exhibited a lower photocurrent ( $60 \mu\text{A cm}^{-2}$ ) than that of the ZnO-CNT hybrid ablated for the same time using the laser with the wavelength of 355 nm photocurrent ( $120 \mu\text{A cm}^{-2}$ ). Thus, the optimal PLA condition to synthesize a ZnO-CNT hybrid with high photocatalytic activity can be determined as 10 min of ablation time using the laser with wavelength of 355 nm. Too long an ablation time induces an inactive photocatalytic phase (i.e., ZnO NP) while insufficient ablation energy may hamper the obtaining of well-dispersed CNTs with a high surface area onto the 2D porous ZnO NS.

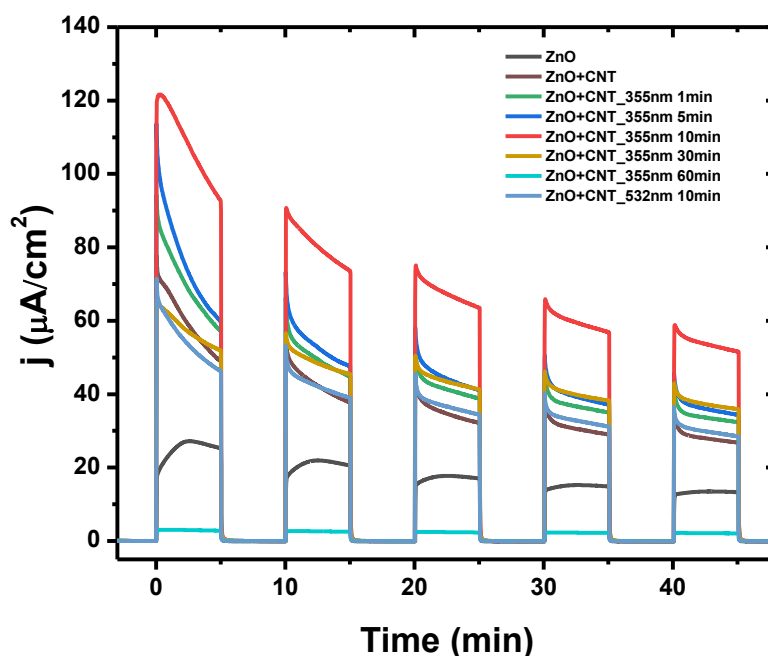


**Figure 8.** Photoelectrochemical measurements showing the transient response of ZnO NS and ZnO NS-CNT hybrids under UV-vis irradiation in a 0.5 M  $\text{Na}_2\text{SO}_4$  electrolyte.

Figure 9 represents UV-vis absorption spectra of the ZnO and ZnO NS-CNT hybrids. A strong absorption at the wavelength shorter than 400 nm was found for all samples related with the intrinsic bandgap absorption of ZnO [5,6,8,12]. Although ZnO generally shows absorption peak near at 380 nm, the absorption peak at 380 nm was not observed for the samples possible due to hybridization effects between nanoporous ZnO nanosheets and nanostructured carbon materials of CNT. Notably, the optical absorption for UV as well as visible light regions was decreased after hybridization with CNTs. Although absorption for the visible light region was slightly increased after hybridization, the absorption for UV region was significantly decreased, as shown in Figure 9. Thus, although precise calculation for the total absorption may be difficult for the ZnO-CNT hybrids, the total absorption may decrease after hybridization. Therefore, the enhanced photocatalytic activities of ZnO NS-CNT hybrids are difficult to be explained by optical properties, indicating that in-depth study on the modulations of electrochemical properties after hybridization via PLA need to be considered.

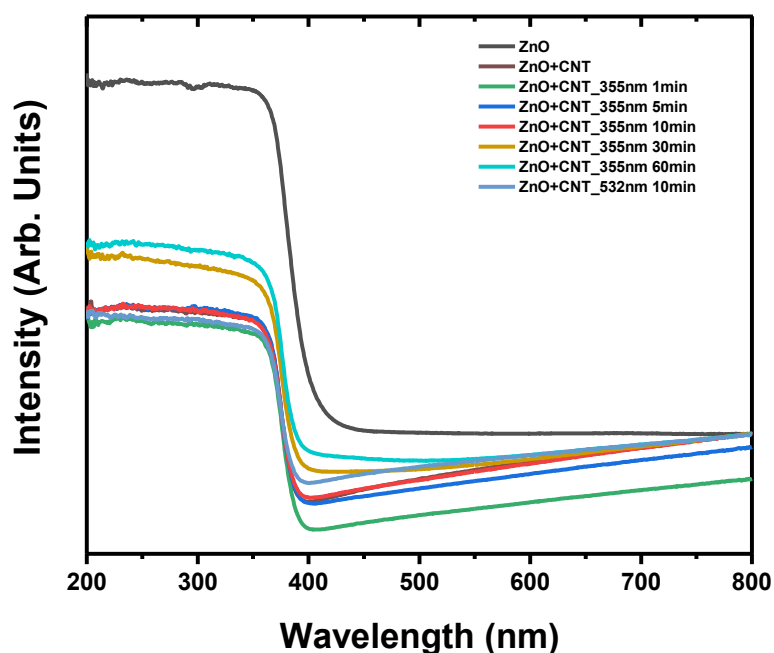


Figure 9. UV-vis absorption spectra of ZnO NS and ZnO NS-CNT hybrids.

Charge transport behavior at the interface between photoanode and electrolyte was investigated by electrochemical impedance spectroscopy (EIS). Nyquist plots of the ZnO NS-CNT hybrids are presented in Figure 10a. Noted that the arc in the Nyquist plot is associated with the charge transfer process at the interface between electrode and electrolyte. Generally, lower interface resistance (i.e., facile charge transfer) is represented as smaller arc radius in the Nyquist plot. ZnO NS-CNT hybrids exhibited substantially lower interface resistance than pristine ZnO NS (Figure 10a), which can be attributed to the high conductivity of CNTs. However, a ZnO NS-CNT hybrid ablated for 60 min showed significantly larger interface resistance than that of ZnO NS (Figure 10b). This indicates that ZnO NPs formed during prolonged ablation may have intrinsically low conductivity (i.e., an insulating phase). In addition, a one dimensional (1D) tubular structure of CNTs is more suitable as a facile charge transport tunnel compared to zero dimensional (0D) GQDs, arising from the complete transformation of CNT to GQD during the prolonged PLA process. These results demonstrated that PLA is an effective tool for hybridizing ZnO NS photocatalysts with conductive CNT while maintaining the advantages of each phase.

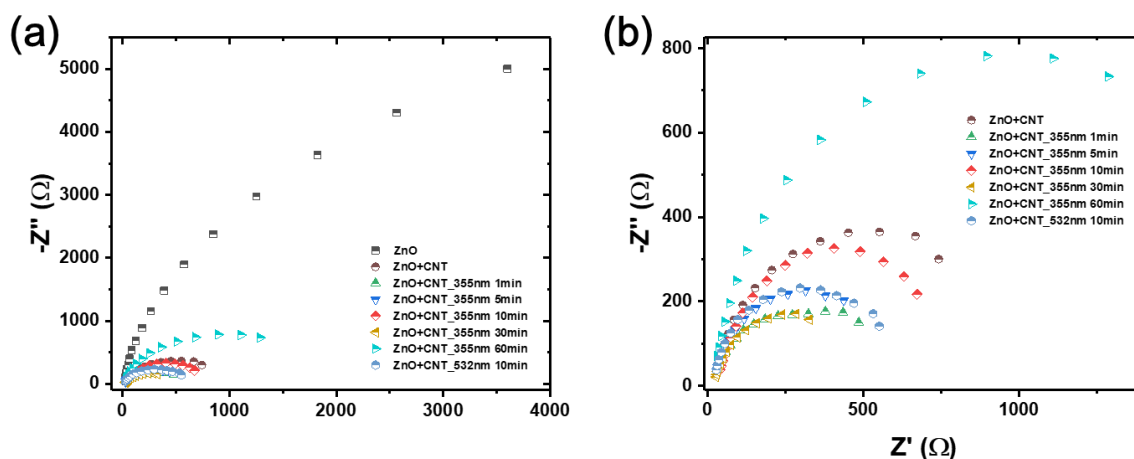


Figure 10. Electrochemical impedance spectroscopy (EIS) spectra of ZnO NS and ZnO NS-CNT hybrids measured (a) in the dark and (b) under light in a 0.5 M  $\text{Na}_2\text{SO}_4$  electrolyte.

### 3. Experimental Section

#### 3.1. Chemical Reagents

All chemicals were purchased from Sigma-Aldrich Inc. and used as is without further purification.

#### 3.2. Synthesis of ZnO NS

0.68 g of ZnCl<sub>2</sub>, 0.3 mL of NH<sub>4</sub>OH, and 0.7 g of hexamethylenetetramine (HMTA) were dissolved in 50 mL of DI water by stirring. The prepared solution was transferred to a Teflon-lined stainless steel autoclave and reacted at 150 °C for 5 h. The product was vacuum filtered and washed with DI water and ethanol for several times. The washed powder was dried in electrical oven at 70 °C under air. The powder was further calcined at 350 °C for 2 h.

#### 3.3. Synthesis of ZnO NS-CNT Hybrids via Pulsed Laser Ablation

In a typical process, 100 mg of ZnO NS and 10 mg of CNT was dispersed in 400 mL of anhydrous ethanol using ultrasonication. A Q-switch ND:YAG laser system was employed at room temperature and in the air. The suspension, which forms a vertical water column, was ablated by a horizontal pulsed laser beam (355 and 532 nm, third harmonic, 10 ns pulse width) at a repetition rate of 20 Hz. The pulsed laser beam was focused to a diameter of around 1 mm with an ablation energy of 0.1 J.

#### 3.4. Structural Characterizations

To investigate morphology of the samples, scanning electron microscopy (SEM; S4800, Hitachi, Tokyo, Japan) was employed. Transmission electron microscopy (TEM; Talos F200X; Thermo Fisher Scientific) equipped with an energy dispersive X-ray (EDX) was also utilized to study structural and compositional characteristics of the samples. For studying crystal structure of the samples, powder X-ray diffraction (XRD) technique was employed using Cu-K $\alpha$  radiation ( $\lambda = 0.15418$  nm) at 40 kV and 100 mA (D/MAX-2500/PC, Rigaku, Tokyo, Japan). The specific surface area of the samples was calculated by nitrogen adsorption-desorption measurements (TriStar II 3020; MicroMetrics, Norcross, GA, USA) and the Brunauer-Emmett-Teller (BET) surface areas of the samples were obtained.

#### 3.5. Photoelectrochemical Characterizations

A standard three-electrode cell was used to measure the photoelectrochemical properties using a potentiostat (Autolab PGSTAT; Metrohm, Herisau, Switzerland). Graphite and standard Ag/AgCl electrodes were used as counter and reference electrodes, respectively. For the working electrodes, 10 mg of sample powder was added to 1 mL of Liquion solution, which was subsequently sonicated for 1 h and stirred overnight. The solution was then spin-coated onto a fluorine doped tin oxide (FTO) glass substrate and dried in an oven (60 °C) overnight. 0.5 M Na<sub>2</sub>SO<sub>4</sub> solution as an electrolyte was prepared for the photoelectrochemical measurements. Xe lamp (300 W, 280–700 nm) was used to irradiate the working electrodes. Electrochemical impedance spectroscopy (EIS) was employed to calculate charge transfer resistance of the samples ( $R_{ct}$ ). The frequency range of 0.01–10<sup>5</sup> Hz under an AC applied voltage of 5 mV was investigated for EIS. Electrochemically active surface area (ECSA) of the samples were calculated by cyclic voltammetry (CV) measured over a potential range from 0.46 to 0.56 V vs. RHE. Based on CV data, the electrochemical double layer capacitance ( $C_{dl}$ ) was calculated. To be specific, scan rates were changed from 20 to 100 mV s<sup>-1</sup> and the difference in current density between anodic and cathodic sweeps ( $\Delta J = J_{anodic} - J_{cathodic}$ ) at the middle of potential range was used to calculate  $C_{dl}$ ; the slope for  $\Delta J$  vs. scan rate plot has linear relationship with the  $C_{dl}$  of sample.

#### 3.6. Optical Property Characterization

UV-visible optical absorption spectra were collected with a V-699 (JASCO) spectrometer (Easton, MD, USA) with a reference of dry-pressed BaSO<sub>4</sub> disk.

#### 4. Conclusions

In summary, we first developed ZnO NS-CNT hybrids using a PLA technique. PLA conditions were optimized to prepare highly active photocatalytic nanocomposites. Specifically, ablation time of about 10 min using the wavelength of 355 nm was selected as the best condition for preparing ZnO NS-CNT hybrids, where 1D CNT with tubular structure is well hybridized with 2D porous ZnO NS. Longer ablation time results in the disappearance of the 1D tubular structure of CNT (i.e., complete transformation into QDs) while insufficient ablation was not able to effectively disperse the CNT aggregates onto the surface of the ZnO NS. The ZnO NS-CNT hybrid exhibited substantially enhanced photocatalytic activity about 4–5 times than the pristine ZnO NS. Hence, these results demonstrate that PLA can be a powerful technique to develop ZnO NS photocatalysts with conductive CNT.

**Author Contributions:** H.H. conceived the project; Y.Y.R. and H.H. designed the experiments; Y.Y.R. prepared the samples; H.H. and T.K. wrote the manuscript; All authors participated in analyzing the data and commented on the manuscript; All authors gave final approval for publication.

**Funding:** This work was supported by the Hongik University new faculty research support fund and the National Research Foundation of Korea (NRF) funded by the Ministry of Science, ICT and Future Planning (2018R1D1A1A02085938).

**Conflicts of Interest:** There are no competing interests for this manuscript.

#### References

1. Li, Q.; Guo, B.D.; Yu, J.G.; Ran, J.R.; Zhang, B.H.; Yan, H.J.; Gong, J.R. Highly Efficient Visible-Light-Driven Photocatalytic Hydrogen Production of CdS-Cluster-Decorated Graphene Nanosheets. *J. Am. Chem. Soc.* **2011**, *133*, 10878–10884. [[CrossRef](#)] [[PubMed](#)]
2. Yin, Z.Y.; Wang, Z.; Du, Y.P.; Qi, X.Y.; Huang, Y.Z.; Xue, C.; Zhang, H. Full Solution-Processed Synthesis of All Metal Oxide-Based Tree-like Heterostructures on Fluorine-Doped Tin Oxide for Water Splitting. *Adv. Mater.* **2012**, *24*, 5374–5378. [[CrossRef](#)] [[PubMed](#)]
3. Zheng, Y.; Jiao, Y.; Ge, L.; Jaroniec, M.; Qiao, S.Z. Two-Step Boron and Nitrogen Doping in Graphene for Enhanced Synergistic Catalysis. *Angew. Chem. Int. Ed.* **2013**, *52*, 3110–3116. [[CrossRef](#)] [[PubMed](#)]
4. Lewis, N.S.; Nocera, D.G. Powering the planet: Chemical challenges in solar energy utilization. *Proc. Natl. Acad. Sci. USA* **2006**, *103*, 15729–15735. [[CrossRef](#)] [[PubMed](#)]
5. Pawar, R.C.; Lee, C.S. Single-step sensitization of reduced graphene oxide sheets and CdS nanoparticles on ZnO nanorods as visible-light photocatalysts. *Appl. Catal. B Environ.* **2014**, *144*, 57–65. [[CrossRef](#)]
6. Qiu, R.L.; Zhang, D.D.; Mo, Y.Q.; Song, L.; Brewer, E.; Huang, X.F.; Xiong, Y. Photocatalytic activity of polymer-modified ZnO under visible light irradiation. *J. Hazard. Mater.* **2008**, *156*, 80–85. [[CrossRef](#)] [[PubMed](#)]
7. Chakrabarti, S.; Chaudhuri, B.; Bhattacharjee, S.; Das, P.; Dutta, B.K. Degradation mechanism and kinetic model for photocatalytic oxidation of PVC-ZnO composite film in presence of a sensitizing dye and UV radiation. *J. Hazard. Mater.* **2008**, *154*, 230–236. [[CrossRef](#)] [[PubMed](#)]
8. Bizarro, M.; Sanchez-Arzate, A.; Garduno-Wilches, I.; Alonso, J.C.; Ortiz, A. Synthesis and characterization of ZnO and ZnO:Al by spray pyrolysis with high photocatalytic properties. *Catal. Today* **2011**, *166*, 129–134. [[CrossRef](#)]
9. Ye, R.Q.; Xiang, C.S.; Lin, J.; Peng, Z.W.; Huang, K.W.; Yan, Z.; Cook, N.P.; Samuel, E.L.G.; Hwang, C.C.; Ruan, G.D.; et al. Coal as an abundant source of graphene quantum dots. *Nat. Commun.* **2013**, *4*, 2943. [[CrossRef](#)]
10. Dong, Y.Q.; Lin, J.P.; Chen, Y.M.; Fu, F.F.; Chi, Y.W.; Chen, G.N. Graphene quantum dots, graphene oxide, carbon quantum dots and graphite nanocrystals in coals. *Nanoscale* **2014**, *6*, 7410–7415. [[CrossRef](#)]
11. Amendola, V.; Meneghetti, M. What controls the composition and the structure of nanomaterials generated by laser ablation in liquid solution? *Phys. Chem. Chem. Phys.* **2013**, *15*, 3027–3046. [[CrossRef](#)] [[PubMed](#)]
12. Kulinich, S.A.; Kondo, T.; Shimizu, Y.; Ito, T. Pressure effect on ZnO nanoparticles prepared via laser ablation in water. *J. Appl. Phys.* **2013**, *113*, 033509. [[CrossRef](#)]
13. Amendola, V.; Meneghetti, M. Laser ablation synthesis in solution and size manipulation of noble metal nanoparticles. *Phys. Chem. Chem. Phys.* **2009**, *11*, 3805–3821. [[CrossRef](#)] [[PubMed](#)]

14. Yang, G.W. Laser ablation in liquids: Applications in the synthesis of nanocrystals. *Prog. Mater. Sci.* **2007**, *52*, 648–698. [[CrossRef](#)]
15. Shi, Y.L.; Pramanik, A.; Tchounwou, C.; Pedraza, F.; Crouch, R.A.; Chavva, S.R.; Vangara, A.; Sinha, S.S.; Jones, S.; Sardar, D.; et al. Multifunctional Biocompatible Graphene Oxide Quantum Dots Decorated Magnetic Nanoplatfom for Efficient Capture and Two-Photon Imaging of Rare Tumor Cells. *ACS. Appl. Mater. Interfaces* **2015**, *7*, 10935–10943. [[CrossRef](#)] [[PubMed](#)]
16. Park, M.; Ha, H.D.; Kim, Y.T.; Jung, J.H.; Kim, S.H.; Kim, D.H.; Seo, T.S. Combination of a Sample Pretreatment Microfluidic Device with a Photoluminescent Graphene Oxide Quantum Dot Sensor for Trace Lead Detection. *Anal. Chem.* **2015**, *87*, 10969–10975. [[CrossRef](#)] [[PubMed](#)]
17. Cushing, S.K.; Li, M.; Huang, F.Q.; Wu, N.Q. Origin of Strong Excitation Wavelength Dependent Fluorescence of Graphene Oxide. *ACS Nano* **2014**, *8*, 1002–1013. [[CrossRef](#)]
18. Deepti, C.; Simrit, S.; Vankar, V.D.; Neeraj, K. ZnO Nanoparticles Decorated Multi-walled Carbon Nanotubes for Enhanced Photocatalytic and Photoelectrochemical Watersplitting. *J. Photochem. Photobiol. A* **2018**, *351*, 154–161.
19. Suneel, K.; Nagappagari, L.R.; Ashish, K.; Muthukonda, V.S.; Venkata, K. Two Dimensional N-doped ZnO-graphitic Carbon Nitride Nanosheets Heterojunctions with Enhanced Photocatalytic Hydrogen Evolution. *Int. J. Hydrogen Energy* **2018**, *43*, 3988–4002.
20. He, W.; Xuan, L.; Shulan, W.; Li, L. Dual Templating Fabrication of Hierarchical Porous Three-dimensional ZnO/carbon Nanocomposites for Enhanced Photocatalytic and Photoelectrochemical Activity. *Appl. Catal. B Environ.* **2018**, *222*, 209–218.
21. Wang, Z.; Luo, C.; Zhang, Y.; Gong, Y.; Wu, J.; Fu, Q.; Pan, C. Construction of Hierarchical TiO<sub>2</sub> Nanorod Array/graphene/ZnO Nanocomposites for High Performance Photocatalysis. *J. Mater. Sci.* **2018**, *53*, 15376–15389. [[CrossRef](#)]
22. Su, Y.; Li, S.; He, D.; Yu, D.; Liu, F.; Shao, N.; Zhang, Z. MOF-Derived Porous ZnO Nanocages/rGO/Carbon Sponge-Based Photocatalytic Microreactor for Efficient Degradation of Water Pollutants and Hydrogen Evolution. *ACS Sustain. Chem. Eng.* **2018**, *6*, 11989–11998. [[CrossRef](#)]



© 2019 by the authors. Licensee MDPI, Basel, Switzerland. This article is an open access article distributed under the terms and conditions of the Creative Commons Attribution (CC BY) license (<http://creativecommons.org/licenses/by/4.0/>).